Earth Planets Space, **62**, 309–318, 2010

Studies of the wind filtering effect of gravity waves observed at Allahabad (25.45°N, 81.85°E) in India

G. K. Mukherjee[1], Pragati Sikha R.[2], N. Parihar[3], Rupesh Ghodpage[3], and P. T. Patil[4]

[1]*Indian Institute of Geomagnetism, Panvel (W), Navi Mumbai 410218, India*
[2]*Department of Physics, Andhra University, Visakhapatnam—500003, India*
[3]*Dr. K.S.K.G.R. Laboratory, IIG, Allahabad—221505, India*
[4]*Medium Frequency Radar, IIG, Shivaji University, Kolhapur, India*

(Received December 11, 2008; Revised September 16, 2009; Accepted November 29, 2009; Online published March 4, 2010)

Well-defined coherent wave sources associated with the passage of short-period gravity waves were observed in all-sky images of OH emission on a total 21 occasions during January to May 2008 at Allahabad (25.45°N, 81.85°E, dip lat ∼16.49°N) in India. The wave motions exhibited similar spatial and temporal properties during each month, but the north-east ward motions were distinctly dominant in April and May 2008. It is a well-known theory that the upward propagating gravity waves may be blocked or absorbed at a critical layer. We have computed the magnitude and direction of atmospheric gravity waves subject to blocking by horizontal winds, i.e., critical layer directional filtering. The HWM-93 model (Hedin *et al*., 1996) was used to compute the two components of neutral wind velocity at Allahabad for the period of observation of gravity waves during March and April 2008. Data from two components of wind velocity were then used to construct the blocking diagrams, which show the directions and apparent phase velocities of wave propagation blocked at a given altitude. The blocking diagrams were then compared with experimental observations of gravity waves in OH airglow to determine the accuracy of the wind model and explain the critical layer theory.

Key words: Gravity waves, critical layer, blocking, wind directional filtering effect, Allahabad, propagation characteristics.

1. Introduction

Low light images of OH hydroxyl bands taken with CCD cameras (Taylor *et al*., 1997; Nakamura *et al*., 1999; Mukherjee, 2003) can provide excellent opportunities for remote sensing of the two-dimensional (2D) evolution of spatial and temporal characteristics of the movement of short-period gravity waves over a large geographical region with great precision. The image data provides vital statistical information on the apparent horizontal phase velocity, direction, wavelength, and period of these waves. This collective body of data together with geographical locations, shape, orientation, and time of displays has been most helpful to researchers investigating the main sources of these waves.

In the troposphere, large-amplitude gravity waves are produced by flow over mountains, severe weather events (fronts, squall lines, etc), convection, jet streams, and other processes. These waves can cause cloud banding and affect the rainfall pattern. They also break, in the same manner as the ocean waves break near the sea shore, producing turbulence which can be a hazard to aircrafts.

Gravity waves which propagate higher up into the atmosphere (e.g., into the stratosphere and mesosphere) grow in amplitude due to decreasing air densities. When gravity waves propagate through the airglow layers, the densities of atoms, molecules, and ions that cause photochemical reactions fluctuate. As a result, the airglow layers show 2D wave patterns. This means that in the horizontal airglow extent, the areas with strong and weak emission intensities change both temporarily and spatially. Consequently, temporal and spatial structures of gravity waves can be mapped by observing the airglow intensity images taken with a sensitive CCD camera, enabling researchers to study the dynamic processes occurring in the mesosphere.

It is well known that both the background wind and energy attenuation have profound effects on the characteristics of upward propagating atmospheric gravity waves (Ding *et al*., 2003). Hines (1960) and Cowling *et al*. (1971) studied the effect of background winds on the gravity ray paths. Both research groups found that changes in the intrinsic frequency of the gravity wave were dependent on the direction of the wind. If the gravity wave propagates along the wind, the intrinsic frequency is shifted downward; when the wave frequency equals to zero, wave energy is lost to the mean flow, a process known as critical coupling. Medioros *et al*. (2003) and Taylor *et al*. (1993) found that winds have a directional filtering effect on propagation of gravity waves.

Preliminary data on gravity waves collected at the Allahabad station (25.45°N, 81.85°E, dip lat ∼16.49°N) in India showed that, in 2008, the preferential direction of wave propagation was towards the north-east in the months of April and May and in the south-west direction in February–March (Pragati *et al*., 2010). Taylor *et al*. (1993) explained

doi:10.5047/eps.2009.11.008

that the apparent asymmetry in the wave propagation direction may be caused by a wave filtering effect that can occur at any height where the horizontal wind velocity along the direction of the horizontal wave vector equals the horizontal phase velocity and the intrinsic frequency is Doppler-shifted to zero. A horizontal surface (r-θ plot) has been constructed at the critical altitude to identify the region where the gravity waves are blocked for upward propagation. Gravity waves propagating within the region would be heavily absorbed by diverse mechanisms (Ryan, 1991), and it would not be possible to observe those with horizontal phase speeds lying outside this region.

We have used the HWM-93 model for computing the two components of the background neutral wind. The model reproduces the mean wind profile for any geographic location on any day and at any time of the year. Here, we present and discuss the use of this model in computing the blocking diagrams for a given site—in this case, Allahabad—for different altitudes. The results of new imaging measurements (Pragati *et al.*, 2010) have been compared with the model computation to study the wind filtering effect on the propagation characteristics of gravity waves. These are the first imaging observations of gravity waves from this latitude region in India.

2. The All-sky Imaging System

The nighttime airglow observations were carried out at Allahabad, using an all-sky imager, between January and May 2008. The all-sky imaging system has three components: an optical system, a detector, and an operating notebook PC (hp). A schematic diagram of the optical layout of the all-sky imager is presented in Fig. 1. The optical system collects light from a 180° field of view with a Mamiya RB fisheye lens that has focal length of 24 mm and a focal ratio of 4. The collected light beam is collimated by a telecentric optical plano-convex lens combination to pass through a narrow-band filter with nearly $\perp$ incidence angles. Six filters were used among six filter positions of a filter drum. The six filters installed in the filter wheel are to allow the transmission of OI 630-nm, OI 557.7-nm, 840-nm, 846-nm, and OH Meinel bands at 720–910 nm and the transmission of background light at 857 nm. The OI filters have 2.0-nm band widths, while the OH filter has blocking between 850 and 870 nm with 87% transparency, with a notch at 868 nm to avoid O_2 (0, 1) atmospheric bands. The maximum altitudes of OI 630.0-nm, OI 557.7-nm, and OH Meinel band emissions are 250, 97, and 87 km, respectively. The collimated beam after the filter (diameter ~69 mm) is fed to a Canon camera lens (50 mm, f/0.95) mounted onto the CCD camera to make an image onto the CCD detector's active image area. The detector is a thermo-electrically cooled CCD camera (PIXIS 512) kept at a temperature of −70° to reduce the thermal noise. The CCD chip has 512 × 512 square pixels of 24 μm. The filter wheel and camera shutter are controlled by a notebook PC (hp) with the Windows XP operating system. WINVIEW software was used.

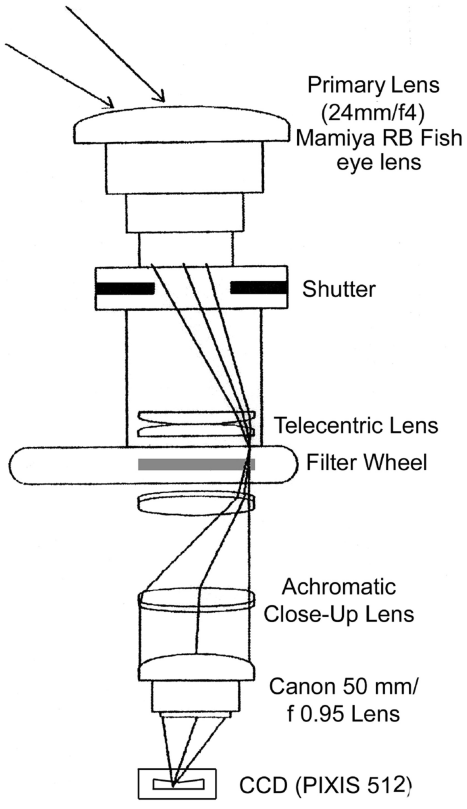

Fig. 1. Schematic of the optical ray paths of the all-sky imager.

3. Image Processing for Spectral Analysis

In this study we defined a gravity wave event as the occurrence of a sequence of airglow images showing wave fronts propagating in a given direction with the bands lasting for more than 30 min. The specific property of the fisheye lens used in this imager is that the distance from the center of the images is proportional to the zenith angles. However, this proportionality is not precise enough to derive the zenith angle directly from the image. Moreover, pixels corresponding to the larger zenith angle are brighter due to the total contribution of the van Rhijn effect, scattering of the atmosphere, lens vignetting, and limb darkening of the lens, among others. The van Rhijn effect is the phenomenon that the line of sight in the airglow layer lengthens with increasing zenith angle; consequently, the airglow intensity at the larger zenith angle becomes stronger if the airglow layer is horizontally homogeneous. This effect must be removed in order to derive airglow intensity perturbations from images. All of these factors should be carefully adjusted for when parameters such as propagation direction, phase velocities, and the horizontal wavelengths of gravity waves are being determined. Initially, the CCD images are processed by subtracting background images and then dividing them by suitable flat field images (Mukherjee, 2003). The nonuniformity of the image due to Van Rhijn effect, atmospheric extinction, and nonuniform sensitivity of the imager at different pixels is roughly corrected by this step. The images obtained with the fisheye lens are transformed into an image in geographic co-ordinates by assuming an altitude of the airglow emission layer. The relationship between the fisheye lens coordinates (expressed by zenith angle θ and the azimuth) and the geographic coordinates (expressed by

Table 1. OH data analysis for February, March, April and May, 2008.

Date	Day number	Wave propagation time (h)	Wave azimuth (±5°)	Observed phase speed (m/s)	Horizontal wavelength (km)
February 03, 2008	34	00:10–00:52	260	43±2	14
February 15, 2008	46	01:21–02:16	30	22±1	13
March 03, 2008	63	00:06–01:19	45 (localized)	10±2	10
March 09, 2008	69	21:50–22:25	220	18±2	10
March 27, 2008 (25)	87	20:00–20:48	260	36±2	37
March 27, 2008 (27)	87	21:26–22:41	300	35±1	34
April 02, 2008	93	20:34–21:55	10	37±2	17
April 07, 2008 OH1	98	20:33–22:54	45	40±2	20
April 10, 2008	101	01:51–02:31	40	12±2	11
April 10–11, 2008	101–102	23:24–00:04	30	31±1	24
April 12, 2008	103	00:40–01:56	15	28±2	15
April 29, 2008	120	01:09–02:31	45	36±1	15
April 30, 2008	121	02:49–03:08	40	48±1	16
May 01, 2008	122	20:05–21:45	20	40±2	20

the horizontal distance r from the station and the azimuth) is given geometrically by Kubota *et al.* (2001) as

$$r = R_{\mathrm{E}}.\alpha$$

and

$$\alpha = \theta - \sin^{-1}(R_{\mathrm{E}}.\sin\theta/(R_{\mathrm{E}} + h_{\mathrm{m}}))$$

where R_{E} is the radius of the earth and h_{m} is the altitude of the airglow emission layer. Coordinate transformation facilitates the measurement of the direction and velocity of movement of airglow structures (Garcia *et al.*, 1997).

In the case presented here, we have converted the fish-eye lens image into an image in geographic coordinates assuming 87 km (h_{m}) to be the altitude of the OH layer. After processing the all-sky images, from a warped image to an unwarped one, the gravity wave parameters, horizontal wavelength, period, phase velocity, and propagation direction are retrieved from successive images by knowing the size of the images transformed into the geographical coordinates and the time difference of two sequential images, respectively (Maekawa, 2000). The imager field of view with 75° zenith angle is 500 km in diameter at an altitude of 87 km.

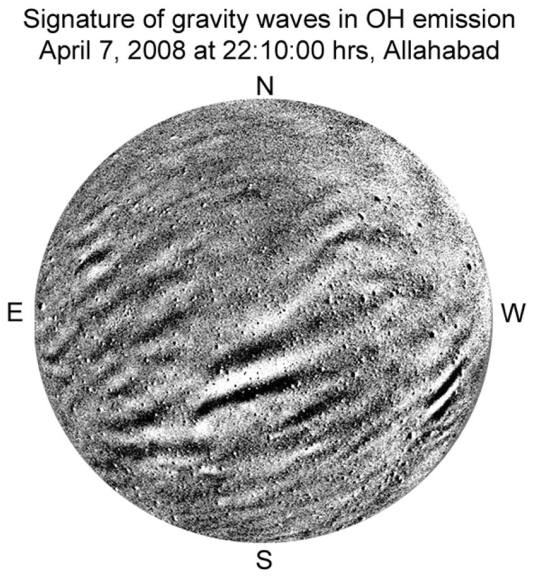

Fig. 2. Signature of gravity waves observed at Allahabad in OH emission on the night of April 7, 2008.

4. Observations and Results

4.1 OH nightglow observations

Nightglow observations of OH Meinel bands (wavelength spread = 550.0 nm–4.4 μm) were carried out at a tropical station, K.S.K.G.R.L. Allahabad, India using an all-sky CCD-based imaging system. The nightglow observations on clear moonless nights centred around the new moon period between 2000 hours and 0500 hours (total observation time: 9 h) on successive days during January, February, March, April, and May, 2008. Wave structure was detected at almost all azimuths up to a range of ∼600 km (limited by the local horizon and assuming emission altitude of 87 km) on 21 occasions during this time. In our study, we analyzed only 16 nights of quality data on the observed gravity wave phenomena, discarding the nightglow observations during this period that were contaminated with clouds. The gravity wave structure showed a well-defined OH-pattern, with near east-west-aligned wave fronts extending over the whole camera field of view. The data were first analyzed to determine the geographic location and orientation of the wave patterns; in doing so, we also determined the horizontal phase speeds and horizontal wavelengths. Then, for each display (assuming the emission height of 87 km), we determined the average horizontal wavelengths and velocities. Some of the results obtained are summarized in Table 1, which lists the azimuth of the wave motions (i.e., the normal to the wave fronts) together with their date, timings, observed phase speeds, and horizontal wavelengths for 14 of the displays recorded (Pragati *et al.*, 2010). It was usually easier to determine the orientation and direction of the motion of the wave pattern than to accurately measure the speed of the wave motions.

4.2 OI 557.7-nm nightglow observations

The gravity waves were also observed in OI 557.7-nm images in April 2009 at the both Kolhapur (India) (16.8°N,

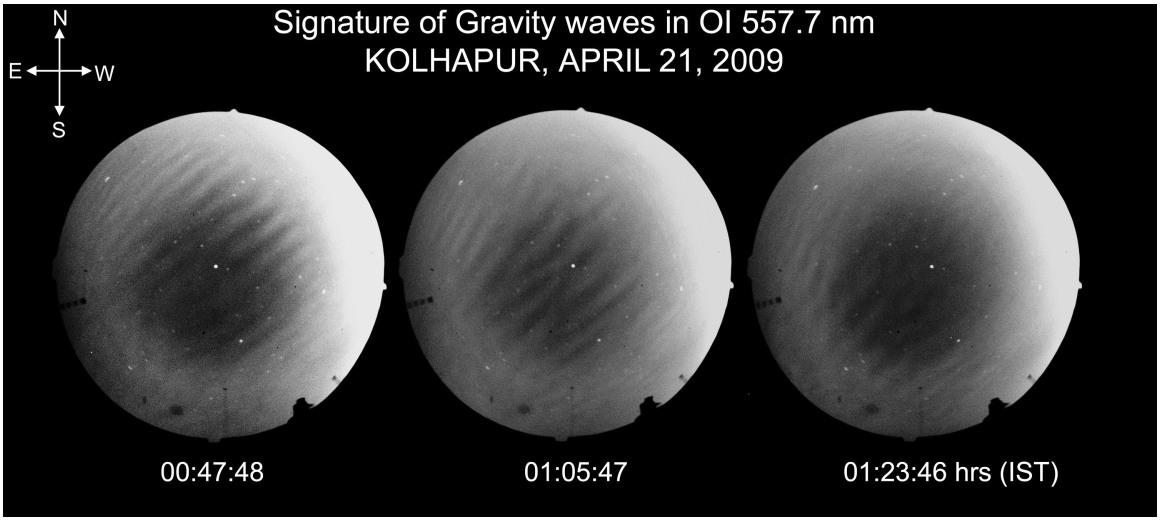

Fig. 3. Signature of gravity waves observed in OI 557.7-nm images on April 21, 2009 at Kolhapur. The image at the center shows an example of wave breaking at 0105:47 hours.

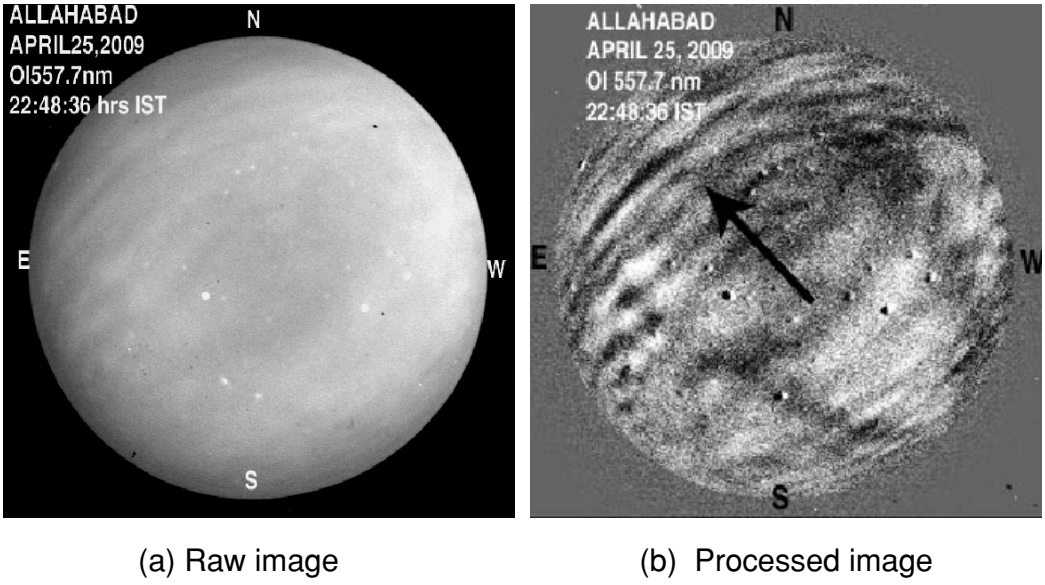

Fig. 4. Signature of gravity waves observed at Allahabad in the OI 557.7-nm images at 22:48:36 hours on the night of April 25, 2009. (a) raw image, (b) processed image.

74.2°E) and Allahabad stations, but these signatures were not recorded in the OI 630.0-nm and OH images. Figure 3 shows three sequential OI 557.7-nm images observed at Kolhapur on the night of April 20–21, 2009. They were spread over a distance of more than 400 km at an altitude of 97 km. The gravity wave fronts were observed to be aligned along the north-west to south-east direction at 00:47:48 hours. At the center of the image, the breaking of the wave fronts can be seen to take place at 01:05:47 hours on April 21, 2009. Thereafter, their propagation in the south-west direction slows down. However, the alignment of the wavefronts changes during the course of night. The wavelengths varied between 30 and 40 km.

Figure 4 shows the signature of gravity waves observed at Allahabad in the OI 557.7-nm images obtained on the night of April 25, 2009. These waves were prominent in the north-east portion of the sky and were moving in the north-east direction. Based on consecutive images, we inferred the phase velocity of the waves to be 50 m/s; the wavelength and periodicity of the waves were 38 km and 13 min, respectively. These values are the signature of short-period atmospheric gravity waves at an altitude of 97 km.

4.3 Wind profiles for the Allahabad station

In the absence of detailed simultaneous wind measurements at the location of our observation site at Allahabad, we chose to use the two wind profiles (meridional component, V_m, and the zonal component, V_z) of average neutral wind velocity from the HWM-93 wind model (Hedin *et al.*, 1996). Other researchers have used a model of the zonal and meridional wind profiles for each month using available climatological information (Forbes, 1982a, b; Fleming *et al.*, 1988; Fleming and Chandra, 1989; Chandra *et al.*,

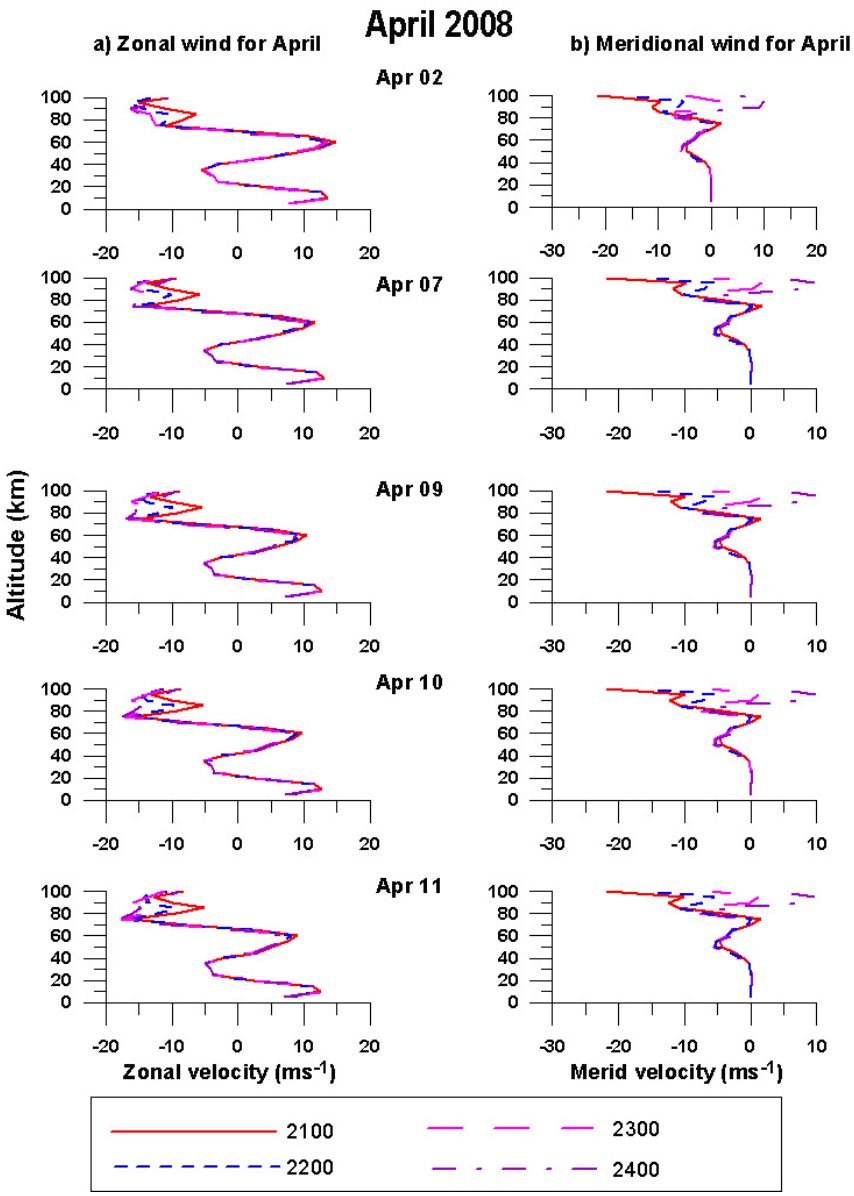

Fig. 5. Two components (zonal and meridional) of wind velocity computed from the HWM-93 model during the period of observation of gravity waves at Allahabad in April 2008 showing the effect of change in the local time as a function of altitude.

1990). The HWM-93 model adopted by us for determining the total velocity component is an empirical model of the horizontal neutral wind (V_m and V_z) in the upper thermosphere. It is based on wind data obtained from the AE-E and DE-2 satellites. A limited set of vector spherical harmonics is used to describe the zonal and meridional wind components. The first edition of the model, released in 1987, was extended for winds above an altitude of 220 km with the inclusion of wind data from a ground-based incoherent scatter radar and Fabry-Perot optical interferometer. HWM-90 was extended down to 100 km and uses mf/meter data; HWM-93 was extended down to the ground solar cycle variations. Variations with magnetic activity (A_p index), including mid- and low-latitude data, are reproduced by the model.

The model describes the transition from predominantly diurnal variation in the upper thermosphere to semi-diurnal variation in the lower thermosphere and the transition from summer to winter flow above 140 km to winter to summer flow below this height. This HWM model provides the components for the zonal and meridional winds for a specified latitude, longitude, time, and A_p index. A comparison of the HWM values with winds derived from IRI parameters and from ionosonde measurements have generally been in good agreement. Figure 5 shows two components (zonal and meridional) of wind velocity computed from the HWM-93 model during the period of observation of gravity waves at 21:00, 22:00, 23:00, and 24:00 hours at Allahabad during April 2008. To examine the effect of changing time on the blocking surfaces in the diagrams, we plotted the zonal and meridional wind profile as a function of altitude at 1-h intervals between 2100 hours and 2400 hours, which is the period during which most of the gravity wave data were recorded. As expected, the zonal winds showed maximum variations below an altitude of 80 km, and minimal changes occurred above 80 km; in contrast, the merid-

ional winds varied substantially. The maximum value for the zonal component of the wind was ∼15 m/s around 60 km, and the maximum value of the meridional component was ∼ −20 m/s around 90 km.

4.4 The model for critical level blocking

The observations revealed the spatial and temporal properties for the wave, but with a distinct tendency toward preferential directions of motion which varied from month to month. The apparent asymmetry in the propagation headings of the gravity waves is due to the presence of critical layers, which can occur at any height level where the horizontal wave vector equals the horizontal phase velocity and the intrinsic frequency is Doppler-shifted to zero. A horizontal surface region can be constructed at the critical layer height to obtain a polar plot ("a blocking diagram") showing the range of azimuthal angles and speeds of gravity waves that are blocked from further upward propagation (Ryan, 1991). Gravity waves with horizontal phase speeds and directions within this region would encounter heavy absorption from a large number of diverse and relatively unstructured mechanisms (Booker and Bretherton, 1967; Hazel, 1967; Jones, 1968; Fritts and Geller, 1976; Fritts, 1978; He *et al*., 1990) as they approach the critical layer. A horizontal surface can be constructed at the critical layer altitude to obtain a polar plot. Gravity waves with horizontal phase velocities outside this region would not encounter any critical layer and should be observable.

The Doppler-shifted frequency, Ω, due to the horizontal wind V_o is given by

$$\Omega = \omega - k_x.V_{ox} \tag{1}$$

where ω is the source frequency, k_x is the magnitude of the horizontal wave vector, and V_{ox} is the component of V_o along wave propagation direction. Equation (1) can be rewritten as

$$\Omega = \omega(1 - V_{ox}/v_x) \tag{2}$$

Where v_x, is the observed horizontal phase speed of the wave. Consequently, at the critical layer, when $V_{ox} \rightarrow v_x$, $\Omega \rightarrow 0$. According to Wang and Tuan (1988), Eq. (2) can be expressed in terms of the zonal and meridional components as

$$\Omega = \omega\left(1 - \frac{V_z \cos\phi + V_m \sin\phi}{v_x}\right) \tag{3}$$

where V_z and V_m are the zonal and the meridional wind components, respectively.

Using the condition given in Eq. (3) defined by $\Omega \leq 0$, the blocking diagrams (forbidden regions) were prepared for each month using two components of wind profile (HWM-93) derived for the Allahabad station with the appropriate parameters (A_p, $F_{10.7\,cm}$ values) during the period of observation of gravity waves at any height below the peak of the OH layer for each propagation direction ϕ and phase speed v_x. Although downward reflection from any critical layer can be significant (He *et al*., 1990), they do not affect the OH layer if the sources are located in the lower atmosphere. Polar plots (blocking diagrams) with v_x as the radius and ϕ as the polar angle were then constructed to determine which directions and magnitudes are blocked in terms of gravity wave propagation up to OH altitudes. As expected, the plot shows the "forbidden" region for wave

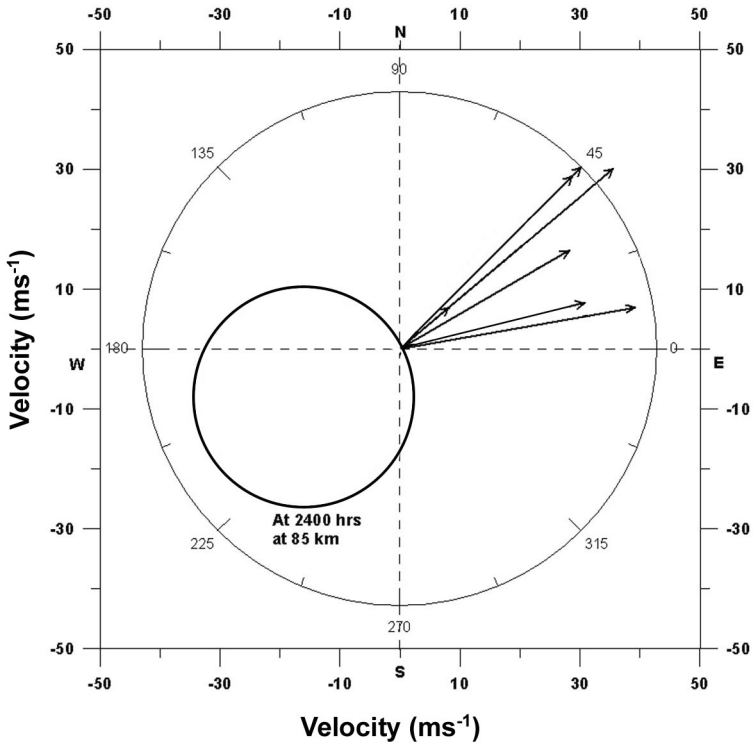

Fig. 6. Blocking diagram for April 2008 at Allahabad. Parameters: altitude, 85 km; time, 24:00 hours.

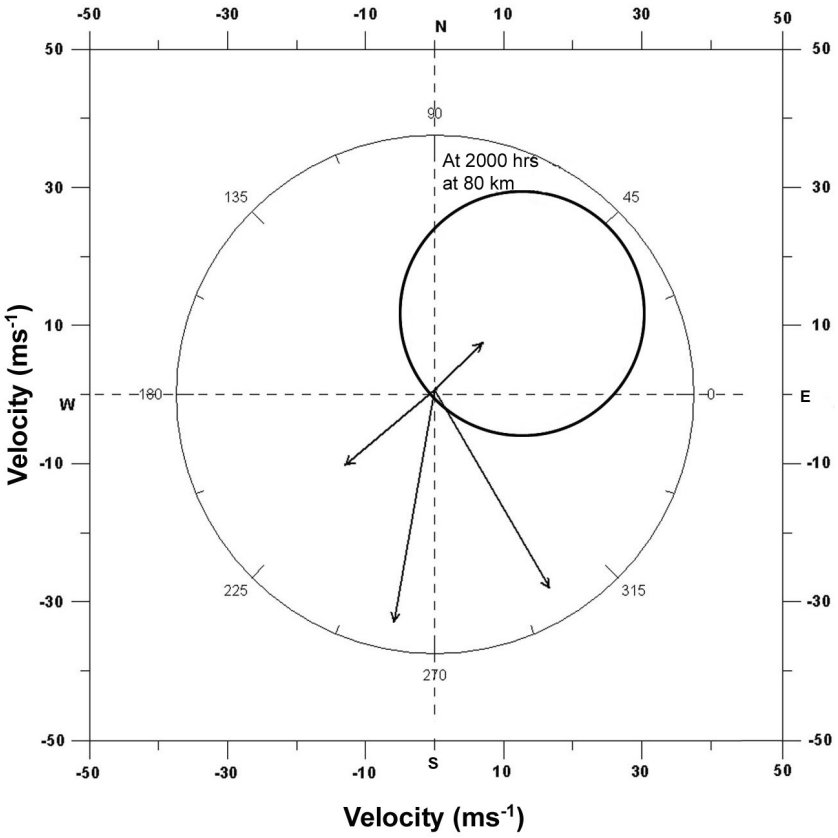

Fig. 7. Blocking diagram for March 2008 at Allahabad. Parameters: altitude, 80 km; time 20:00 hours.

propagation due to the strong winds in the stratosphere and lower mesosphere. The blocking region restricts all propagating gravity waves with observed phase speeds below a critical value.

Figure 6 shows the blocking diagram for April at local midnight for the observation site. The figure was computed for a height of 85 km, which is just below the nominal peak of the OH emission (∼87 km, thickness 8 km), and the plot therefore represents the cumulative effects of wave blocking for all heights up to and including the base of the OH layer. The circular nature of the plot indicates the restricted regions for wave propagation. Added to this plot is another polar plot which represents the horizontal propagation direction of gravity waves in the north-east direction along with their magnitudes recorded during the month of April.

In March, four wave displays and four velocity measurements were made (see Table 1). Figure 7 represents the blocking diagram for the month of March. It can be seen that the waves propagate in the north-east direction for only one day; for the remaining three days of observation the propagation is in the south-west direction. On two occasions (March 2 and 4), localized gravity waves were observed. The horizontal phase velocity and horizontal wavelength could not be determined on March 4 because the image obtained was faint.

5. Discussion

The spatial and temporal properties of the wave motions observed are typical of the low-latitude nightglow displays. These displays have occassionally been observed with a time period of <19 min and having a horizontal phase velocity <48 m/s and a horizontal wavelength <39 km. Although individual sources for the waves have been difficult to locate, there are a number of factors that satisfactorily explain the sources. There is almost a complete agreement between the image measurements and the model predictions, and between the predicted and observed directions of wave propagation. This agreement suggests that the middle atmospheric winds can play an important role in governing the flux and azimuthal propagation distribution of short-period wave energy reaching the upper atmosphere.

Figure 8 shows the changes in wave blocking surfaces can occur at different times. Changes in the blocking area during the nighttime may therefore affect the propagation of some of the waves. It is obvious from the plot that the area of the blocking region increases as time advances from 20:00 hours to 24:00 hours. The maximum blocking area was found for 24:00 hour. Thus, changes in the blocking area during the course of night can affect the propagation of some waves, although there is no sign of this in our limited data set. Most of the observed propagation direction was outside the blocking region. Figure 9 shows a 3-D blocking diagram from an altitude of 20 to 100 km at 22:00 hours at Allahabad: both the area and the location of the blocking diagram change as the wave propagates upward from the

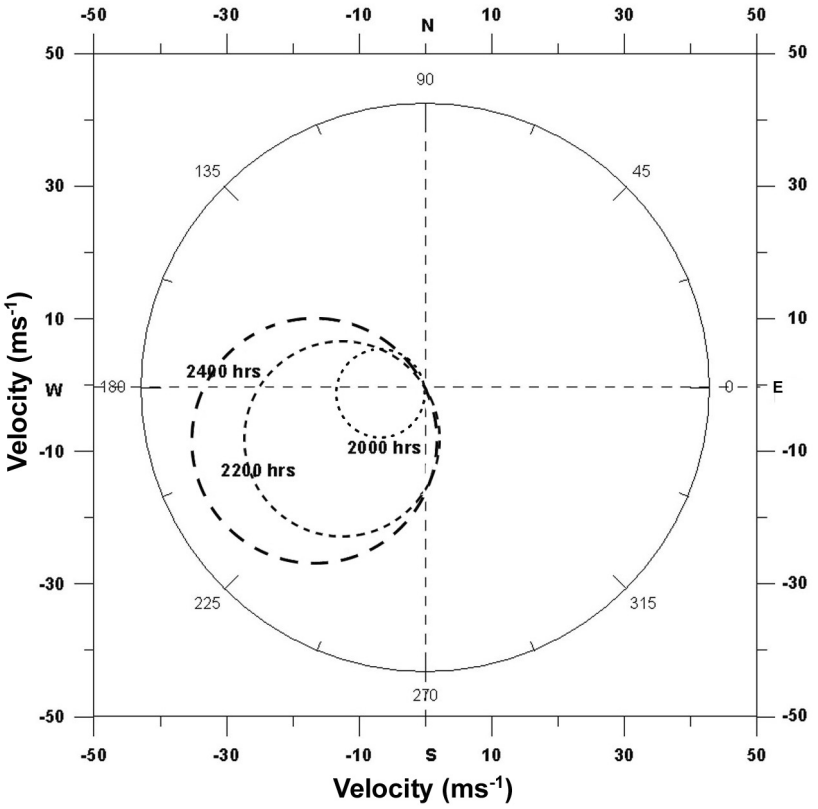

Fig. 8. Blocking diagram for April at 85 km, showing the effects of changing time on the blocking area of the plot.

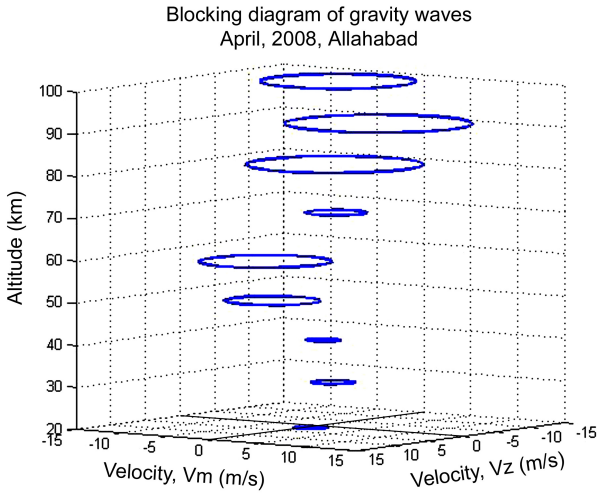

Fig. 9. Three-dimensional blocking diagram from an altitude of 20 to 100 km for April, 2008 at 22:00 hours.

lower atmosphere. It is possible that some of the waves may survive the critical layers and reach higher altitudes.

The two factors which govern the wave propagation direction in the mesopause region are (1) its source location in the lower atmosphere relative to the observer and (2) the background mean wind field in the stratosphere and mesosphere. Gravity waves propagating upward from the lower atmosphere are absorbed into the mean flow as they approach a critical layer where the intrinsic frequency of the wave is Doppler-shifted to zero. This situation may occur at any height when the local horizontal wind speed along the direction of propagation equals the apparent horizontal phase speed of the gravity wave. Gravity waves with horizontal phase velocities outside of this region would not meet, by chance, a critical layer and should be observable. The absence of waves toward the south-west in April indicates that there was little wave source to the north-east of the observer.

There are many sources of gravity waves. One of the most important sources suggested for the wave generation mechanism is the tropospheric convention (Taylor and Hapgood, 1988; Medeiros *et al.*, 2004a, b). As the preferential directions of wave propagation were found to be mainly towards the north and north-east in April and May at the Allahabad observation site, one can assume that the generation source of the gravity waves should be over the continent 250–300 km away in the south and south-west direction. Some of the waves could be also be produced from ducting and/or from waves generated in situ due to reflection at the mesopause. Nakamura *et al.* (2003) reported that the propagation direction of short-period gravity waves at the low-latitude MLT region was consistent with the spatial distribution of tropospheric clouds. Based on a study of imaging observations carried out in Indonesia, Nakamura *et al.* (2003) reported that the propagation direction of the observed gravity waves was closely associated with the cloud distribution and that the observed gravity waves correlated well with the horizontal distribution of GSM images. Nakamura *et al.* (1988) and Taylor and

Hapgood (1988) also identified thunderstorms as a source of short-period gravity waves.

6. Summary and Conclusions

Atmospheric gravity waves play an important role in the dynamics and energetics of the mesosphere, thermosphere, and ionosphere. To understand these wave phenomena we carried out imaging observations with a CCD-based All-sky imager at Allahabad and Kolhapur on clear moonless nights between January and May 2008 and in April 2009. The characteristics of the horizontal propagation parameters (time period, phase velocity, and wavelength) of the gravity waves have been inferred from OH and OI 557.7-nm images. The effect of attenuation or the filtering of gravity waves by neutral wind flow has been also studied.

(1) The theory of gravity wave absorption at critical layers is well-developed. Gravity waves propagating energy upward from the lower atmosphere are absorbed into the mean flow as they approach the critical layer where the intrinsic frequency of the wave is Doppler-shifted to zero. Gravity waves can propagate upwards only when the propagation direction of gravity wave is opposite to the neutral wind direction. All-sky images of the near-infrared OH emission is well suited for this study as they provide reasonable estimates of the direction of motion and the apparent speed of the waves reaching the upper atmosphere. The observations reported here show very good agreement between the observed and the permitted wave azimuths and speeds. For the month of April 2008, the blocking region was in south-west direction, and the waves were propagating towards the north-east direction. The anisotropy in propagation direction in March and April may be due to a wave-filtering effect, which is in agreement with the findings of Taylor *et al*. (1993). The blocking region also varied as a function of time and altitude. There is, however, an overall consistency between the observed GW propagation and the blocking diagrams. The theory of the filtering effect of a gravity wave by its absorption into the mean wind flow at a critical layer is valid only when the background wind through which wave is propagating is somewhat stable (Richardson's number, Ri, of the background medium is greater than $1/4$). When there is a steep vertical gradient of wind flow, wind profiles may become unstable, causing refraction or over-reflection of the upward propagating gravity wave (Taylor *et al*., 1993).

(2) As most of the wave propagation was in the north-east direction, it is possible that for few months each year the direction is reversed and waves may propagate in other directions (south-west). Thus, in order to obtain a lucid understanding of the gravity wave propagation throughout the year, we need a larger data base. It is important to have a large number of measurements of gravity waves spanning different months at the observation site, Allahabad, to confirm the findings of the current wave filter theory. This would enable the apparent change in the drift speed directions to be studied for both the summer and winter period. In future studies, it may also be possible to study the signature of gravity wave simultaneously in OI 557.7-nm emissions (∼97 km). The OI data can provide support and evidence for wave filtering by winds. Sun *et al*. (2007) recently studied the filter effects of the background winds on the propagation of gravity waves using a 3D transfer function model. They concluded that the gravity waves travel easily in the anti-windward direction, primarily because the propagation distance of gravity wave packets along the winds is longer than that against the winds. This leads to a higher energy loss when gravity waves are propagating along the winds than against the winds in the same altitude range. The results showed that the atmospheric winds may act as a directional filter that would permit gravity wave packets propagating against the winds to reach evene ionospheric height with a minimum energy loss and minimum travel time. Therefore, with directional filtering by the winds, the action of the atmospheric processes seems to favor those gravity wave packets that take the minimum time to reach the ionosphere. Other components of gravity waves are also filtered by the viscosity and thermal conduction of the atmosphere as well as by the background winds when the gravity waves propagate upward to higher altitudes.

Acknowledgments. The Department of Science and Technology (DST), Govt. of India, New Delhi funded the research in Upper Atmospheric Sciences in IIG. The night airglow observations at Kolhapur were carried out under the scientific collaboration program (MoU) between IIG, Panvel, and Shivaji University, Kolhapur.

References

Booker, J. R. and F. P. Bretherton, The critical layer for internal gravity waves in a shear flow, *J. Fluid Mech*., **23**, 513–520, 1967.

Chandra, S. E., E. Fleming, M. Schoeberi, and J. J. Barett, Monthly mean global climatology of temperature, wind, geo potential height, and pressure for 0-120 km, *Adv. Space Res*., **10**(6), 3–12, 1990.

Cowling, D. H., H. D. Webb, and K. C. Yeh, Group rays of internal gravity waves in a wind-stratified atmosphere, *J. Geophys. Res*., **76**, 213–220, 1971.

Ding, F., W. Wan, and H. Yuan, The influence of background winds and attenuation on the propagation of atmospheric gravity waves, *J. Atmos Terr. Phys*., **65**, 857–869, 2003.

Fleming, E. and S. Chandra, Equatorial zonal wind in the middle atmosphere derived from geo potential height and temperature data, *J. Atmos. Sci*., **46**(6), 860–866, 1989.

Fleming, E., S. Chandra, M. Shoeberi, and J. Barnett, Monthly mean global climatology of temperature, wind, geo potential height, and pressure for 0-120 km, *NASA Tech. Memo. 100697*, 1988.

Forbes, J. M., Atmospheric tides, 1. Model description and results for the solar diurnal component, *J. Geophys. Res*., **87**(A7), 5222–5240, 1982a.

Forbes, J. M., Atmospheric tides, 2, the solar and lunar semi diurnal components, *J. Geophys. Res*., **87**(A7), 5241–5252, 1982b.

Fritts, D. C., The nonlinear gravity wave critical level interaction, *J. Atmos. Sci*., **35**, 397–413,1978.

Fritts, D. C. and M. A. Geller, Viscous stabilization of gravity wave critical level flows, *J. Atmos. Sci*., **33**, 2276–2284, 1976.

Garcia, F. J., M. J. Taylor, and M. C. Kelly, Two dimensional spectral analysis of mesospheric airglow image data, *Appl. Optics*, **36**(29), 7374–7385, 1997.

Hapgood, M. A. and M. J. Taylor, Analysis of gravity wave image data, *Ann. Geophys*., **8**, 805–813, 1982.

Hazel, P., The effect of viscosity and heat conduction on internal gravity waves at a critical layer, *J. Fluid Mech*., **30**, 775–786, 1967.

He, F., T. F. Tuan, R. Picard, and J. Isler, Optical model analysis of gravity waves reflection from critical layers, *EOS Trans. AGU*, **71**, 1495–1496, 1990.

Hedin, A. E., E. L. Fleming, A. H. Manson, F. G. Schmidlin, S. K. Avery, R. R. Clarck, S. J. Franke, G. J. Fraser, T. Tsuda, F. Vial, and R. A. Vincent, Empirical wind model for the upper, middle and lower atmosphere, *J. Atmos. Terr. Phys*., **58**, 1421–1427, 1996.

Hines, C. O., Internal atmospheric gravity waves at ionospheric heights, *Can. J. Phys*., **38**, 1441–1481, 1960.

Jones, W. L., Reflection and stability of waves instably stratified fluids with shear flow: A numerical study, *J. Fluid Mech*., **34**(3), 609–624, 1968.

Kubota, M., H. Fukunishi, and S. Okano, Characteristics of medium and large scale TIDs over Japan derived from OI 630 nm nightglow observation, *Earth Planets Space*, **53**, 741–751, 2001.

Maekawa, R., Observations of gravity waves in the mesopause region by multicolor airglow imaging, Master Thesis, Kyoto University, 2000.

Medeiros, A. F., M. J. Taylor, H. Takahashi, P. P. Batista, and D. Gobbi, An investigation of gravity wave activity in the low-latitude upper mesosphere: propagation direction and wind filtering, *J. Geophys. Res*., **108**(D14), 4411–4419, 2003.

Medeiros, A. F., R. A. Buriti, E. A. Machado, M. J. Taylor, H. Takahashi, P. P. Batista, and D. Gobbi, Comparison of gravity wave activity observed by airglow imaging from two different latitudes in Brazil, *J. Atmos. Sol. Terr. Phys*., **66**(6–9), 647–655, 2004a.

Medeiros, A. F., H. Takahashi, P. P. Batista, D. Gobi, and M. Taylor, Observation of atmospheric gravity waves using airglow all-sky CCD imager at Cachoeira Paulista (23.1°S, 45.1°W), *Geofísica Int*., **43**(1), 29–39, 2004b.

Mukherjee, G. K., The signature of short period gravity waves imaged in OI 557.7 nm and near infrared OH nightglow emissions over Panhala, *J. Atmos. Sol. Terr. Phys*., **65**, 1329–1335, 2003.

Nakamura, T., T. Tsuda, R. Maekawa, M. Tsutsumi, M. J. Taylor, and M. A. Hapgood, Identification of a thunderstorm as a source of short period gravity waves in the upper atmospheric nightglow emission, *Planet Space Sci*., **36**, 975–985, 1988.

Nakamura, T., A. Higashikawa, T. Tsuda, and Y. Matsushita, Seasonal variations of gravity wave structures in OH airglow with a CCD imager at Shigaraki, *Earth Planets Space*, **51**, 897–906, 1999.

Nakamura, T., T. Aono, T. Tsuda, A. G. Admiranto, E. Achmad, and Suranto, Mesospheric gravity waves over a tropical convective region observed by OH airglow imaging in Indonesia, *Geophys. Res. Lett*., **30**(17), 1882–1885, 2003.

Pragati Sikha, R., N. Parihar, Rupesh Ghodpage, and G. K. Mukherjee, Observations of Gravity Waves in the upper mesosphere region by near infrared Airglow Imaging, *Current Sci*., **98**(3), 392–397, 2010.

Ryan, E. H., Critical layer directional filtering of atmospheric gravity waves: A comparison of airglow observation and a wind profile model, M.Sc. thesis, The University of Cincinnati, Ohio, 1991.

Sun, L., W. Wan, F. Ding, and T. Mao, Gravity wave propagation in the realistic atmosphere based on a three dimensional transfer function model, *Ann. Geophys*., **25**, 1979–1986, 2007.

Taylor, M. J. and M. A. Hapgood, Identification of a thunderstorm as a source of short period gravity waves in the upper atmospheric nightglow emission, *Planet Space Sci*., **36**, 975–985, 1988.

Taylor, M. J., E. H. Ryan, T. F. Tuan, and R. Edwards, Evidence of preferential direction of gravity wave propagation due to wind filtering effect in the middle atmosphere, *J. Geophys. Res*., **98**, 6047–6057, 1993.

Taylor, M. J., W. R. Pendleton Jr., S. Clark, H. Takahashi, D. Gobbi, and R. A. Goldberg, Image measurements of short-period gravity waves at equatorial latitudes, *J. Geophys. Res*., **102**(D22), 26,283–26,299, 1997.

Wang, D. Y. and T. F. Tuan, Brunt Doppler ducting of small-period gravity waves, *J. Geophys. Res*., **93**(A9), 9916–9926, 1988.

G. K. Mukherjee (e-mail: gkm@iigs.iigm.res.in), Pragati Sikha R., N. Parihar, R. Ghodpage, and P. T. Patil